Hierarchical multiscale modeling of polymer-solid interfaces: atomistic to coarse-grained description, and structural and conformational properties of polystyrene-gold systems

Karen Johnston and Vagelis A. Harmandaris

Original Citation:

Johnston, Karen and Harmandaris, Vagelis A.

(2013)

Hierarchical multiscale modeling of polymer-solid interfaces: atomistic to coarse-grained description, and structural and conformational properties of polystyrene-gold systems.

Macromolecules.

ISSN 0024-9297

(Submitted)

This version is available at: http://preprints.acmac.uoc.gr/180/
Available in ACMAC's PrePrint Repository: March 2013

Hierarchical multiscale modeling of polymer-solid interfaces: atomistic to coarse-grained description, and structural and conformational properties of polystyrene-gold systems.

Karen Johnston[*,†] and Vagelis Harmandaris[*,‡,¶]

Max Planck Institute for Polymer Research, Ackermannweg 10, 55128 Mainz, Germany, and Department of Applied Mathematics, University of Crete, GR-71409 Heraklion, Crete, Greece

E-mail: johnston@mpip-mainz.mpg.de; vagelis@tem.uoc.gr

Abstract

A hierarchical simulation approach was developed in order to study polystyrene films sandwiched between two parallel Au(111) surfaces. The coarse-grained potentials describing the interaction of polystyrene with the gold surface were developed systematically using constrained all-atom molecular simulations of a styrene trimer on the Au(111) surface. The model was validated by studying a 5 nm film of short (10mer) polystyrene chains using all-atom and coarse-grained molecular dynamics simulations. The density, structure and conformational properties of coarse-grained films were found to be in excellent agreement with all-atom ones. The coarse-grained model was then used to study the structural and conformational properties of roughly 10 nm and 20 nm thick films with 10, 50, 100 and 200mer chains. The width of the

[*]To whom correspondence should be addressed
[†]Max Planck Institute for Polymer Research, Ackermannweg 10, 55128 Mainz, Germany
[‡]Department of Applied Mathematics, University of Crete, GR-71409 Heraklion, Crete, Greece
[¶]IACM FORTH, GR-71110 Heraklion, Crete, Greece

interphase region of the polymer films is property specific. The density profiles reached the bulk value around 1.5 nm from the interface, for all chain lengths. An estimate of the width of the interphase region based on the conformation tensor profile indicates that the interphase width is proportional to the square root of the chain length (number of monomers) and for 200mer chains the interphase width is approximately 6-9 nm.

Introduction

Polymer thin films are encountered in a variety of different technological applications including adhesives, paint, lubricants and multi-phase composite materials. The overall performance of such materials depends on the polymer properties close to the interface. Nowadays, the design of functional materials used in different applications, such as organic electronics or miniaturized devices, often involves polymer–solid interfaces.[1,2] Due to this broad spectrum of technological applications the properties of polymer–solid interfaces is a very intense research field. Various experimental approaches have been used to study the structural and dynamical properties at a solid surface.[3–6] In addition, a range of simulation methodologies have been employed to study the effect of the interface on the polymer properties. The challenge in simulating these systems is the large range of time and length scales involved and a multiscale modelling approach is necessary. This is an inherent problem in all macromolecular materials since it is related to the different characteristic time scales associated with the motion of different parts of the chain from femtoseconds for bond vibrations up to seconds for long polymer chain relaxations near the glass transition temperature.[7]

Atomistic simulations have the advantage of a detailed all-atom representation of the hybrid material and, therefore, a direct quantitative comparison can be made between the predicted properties and experimental quantities.[8–10] However, the main problem related with the application of atomistic techniques on polymeric materials is the long relaxation times required for equilibration. For polymer–solid systems even longer time scales are involved due to the presence of the solid surface, which might slow the polymer dynamics even further.[8,11–13] In order to reach longer simulation times, systematic coarse-grained models have been developed for various macro-

molecules,[14–16] where the main idea behind such models is to group chemically connected atoms into "superatoms" and derive the effective CG interaction potential (free energy) by taking into account the atomistic details of the particular polymer. To date, there are only a few systematic CG studies of polymer–solid systems. For example, the interaction of polycarbonate near a solid surface has been studied by combining *ab-initio* calculations, describing the interaction of fragments of the polymer with the surface, with CG molecular dynamics.[17,18]

The present work is a part of a systematic approach that hierarchically links together different levels of description starting from the quantum-level through the atomistic level and to the coarse-grained level. Our primary goal is to study a realistic polymer–solid interfacial system and predict its properties directly from the molecular structure. In previous work, we studied polystyrene–gold systems using atomistic simulations, where the interface potentials were obtained from density functional theory (DFT) calculations of small PS fragments. The adsorption energy of the fragments on a gold surface as a function of distance from the surface, for various adsorption sites and molecular orientations[13,19] was used to parameterise a classical force field for the PS–Au interaction that describes accurately all the DFT data. In this work we systematically derive a CG potential for the PS–Au interface and use it to model PS chains with larger molecular weight. We start by developing coarse-grained surface potentials, which are based on the atomistic sampling of oligomers on the surface. The CG potentials are then validated by comparing atomistic and coarse-grained simulations of a short-chain polystyrene melt on gold. Finally, systems with longer-chain polymers are investigated and density profiles, structure and conformations of such systems are analyzed.

Method

The proposed methodology involves the development of a rigorous CG PS–Au interaction potential based on atomistic (AA) data, which were in turn based on DFT calculations.[13,19] All AA and CG simulations were performed using GROMACS 4.5.[20] Details about the atomistic simulations and

forcefield can be found elsewhere.[13,21] For this study a previously developed CG model for PS was used.[16,22] In this model a monomer is represented by two beads, which we denote E (the ethylene backbone group) and P (the phenylene side group), see Figure 1. This model is capable of describing quantitatively the structure, dimensions and conformations of PS chains in the bulk. Here, we extend this model in order to describe the PS–Au interaction. In the present case, the CG systems consist of five different atactic chain types e.g. a 50 chain system has 10 chains of each chain type. The bulk CG systems were setup by placing linear polymer chains in a large box. The chains were relaxed using energy minimisation and soft-core potentials and this was followed by an NpT simulation with $p = 1$ atm and $T = 500$ K until the bulk density was reached.

If we were interested in obtaining the effective CG interaction between a simple molecule (e.g. benzene) and a solid surface then we would directly calculate the potential of mean force (PMF) between the molecule and the solid surface. However, for the case of a macromolecular chain we must consider the fact that the CG bead belongs in a polymer chain and, indeed, the set of the allowed conformations will be different in the latter case. Therefore, to mimic the polymer chain we calculate the PMF for the CG beads using a PS oligomer. The CG PS–Au interactions for each bead type must be developed independently. The bead types are shown in Figure 1 and are described in more detail in the supplementary information.

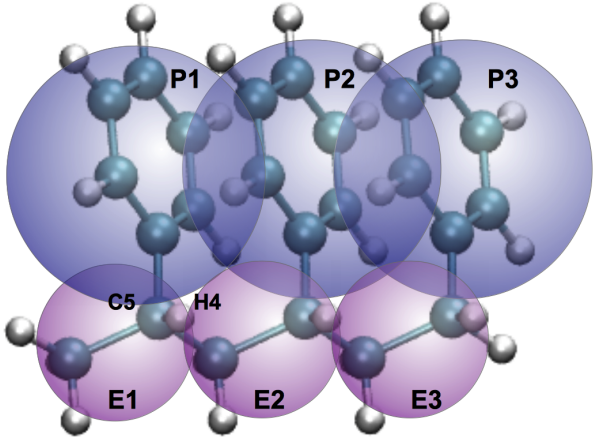

Figure 1: CG bead labelling for surface interaction of a PS isotactic trimer. Atoms C5 and H4 in the picture belong to E1 in the surface interaction.

At the coarse-grained level the interaction between the polystyrene and the surface is repre-

sented by a z-dependent wall potential. Clearly, this approach neglects the structure of the surface, however, in the case of the Au(111) surface the site dependence of the PS–Au interaction is rather weak,[13] which to an extent justifies this approach. Nevertheless, the frictional properties of the surface will be different, which will affect the dynamical behaviour of the polymer at the surface. This will be the subject of a future study.

For the effective potential calculations we used a procedure based on a single PS oligomer near the surface. A similar method was used previously in a study of bulk PS in order to develop the non-bonded CG interaction between CG beads in the bulk.[16] For the bulk case, the effective interaction between the two CG beads at a fixed distance, r, was computed via the constraint force required to keep the two CG beads at this specific distance. In the present case, a single PS oligomer is placed near the gold surface and the system is run, keeping the centre of mass of the group of interest fixed at a particular distance, z, from the surface. The group was placed every 0.05 nm in the range $z_1 = 0.25$ nm up to $z_2 = 1.5$ nm and each simulation was run for 10 ns with output every 0.1 ps. The average constraint forces, f_c, were integrated using the trapezium rule to give the PMF

$$V_{\mathrm{PMF}}(z) = -\int_{z_1}^{z_2} [\langle f_c \rangle_z]\, dz \tag{1}$$

The simulation is repeated, using the same trajectory file, with the interactions between the constrained group and the surface atoms turned off to obtain $V_{\mathrm{PMF,excl}}(z)$. The effective potential for the constrained group with the surface is obtained by subtracting the excluded-interaction PMF from the full-interaction PMF

$$V_{\mathrm{eff}}(z) = V_{\mathrm{PMF}}(z) - V_{\mathrm{PMF,excl}}(z). \tag{2}$$

For the simulations of 10mer PS on Au the simulation boxes were hexagonal with $a = b =$ 4.616 nm, corresponding to 16×16 surface unit cells. For the longer chain systems a larger surface was used so that the sides of the simulation cell were all longer than the ensembled averaged end-to-end distances. For the 50, 100 and 200mer systems axis of length 6.347, 9.232 and 12.694 nm for

the 100-mer systems. These axis are integer multiples of the surface unit cell, which is important so that the CG system can later be backmapped back to the atomistic system. The surface interaction is set up using wall potentials at the bottom and top of the box in z-direction and periodic boundary conditions in the xy-plane. A time step of 1 fs was used for all systems unless otherwise stated. The 10mer systems were equilibrated by running the simulations until the bulk density is reached and then allowing the end-to-end vectors to decorrelate before taking statistics. Equilibration of long polymer chains is a non trivial issue and this will be discussed in a later section.

Development of the coarse-grained polymer–surface potentials

In this part we describe the development of the interaction potential between the CG beads and the Au solid layers as a function of the length of the PS oligomer. We further study the effect of tacticity on the derived potential by using pure stereoregular (isotactic and syndiotactic) PS sequences. Note that the PS–Au interaction developed here includes entropic (temperature) effects as all interactions in the CG description are derived from PMFs (free energies). This is in contrast with CG potentials developed in the past using ab-initio data, which are based on the ground state (zero temperature) potential energy.[17,18] The latter approach is expected to be a reasonable approximation of the interface potential as long as the CG superatom–surface interaction is enthalpy dominated i.e. very strong compared to the thermal energy. The current approach explicitly accounts for entropy, which is expected to be very important for soft matter systems, thus being applicable to all soft–hard matter interfaces.

Effect of the oligomer length

The first issue to be addressed is the length of the oligomer necessary to obtain realistic sampling of the allowed conformations. To determine this we calculated effective potentials using a 3mer, a 5mer and a 7mer for an isotactic chain. The beads at the chain ends will not interact with the surface in the same way as those in the middle of the chain and it is important to differentiate

between these beads. Since the central beads are more likely to be affected by the surrounding chain we have considered the central beads rather than the beads at the chain ends. The results for isotactic 3-, 5- and 7mer chains are shown in Figure 2.

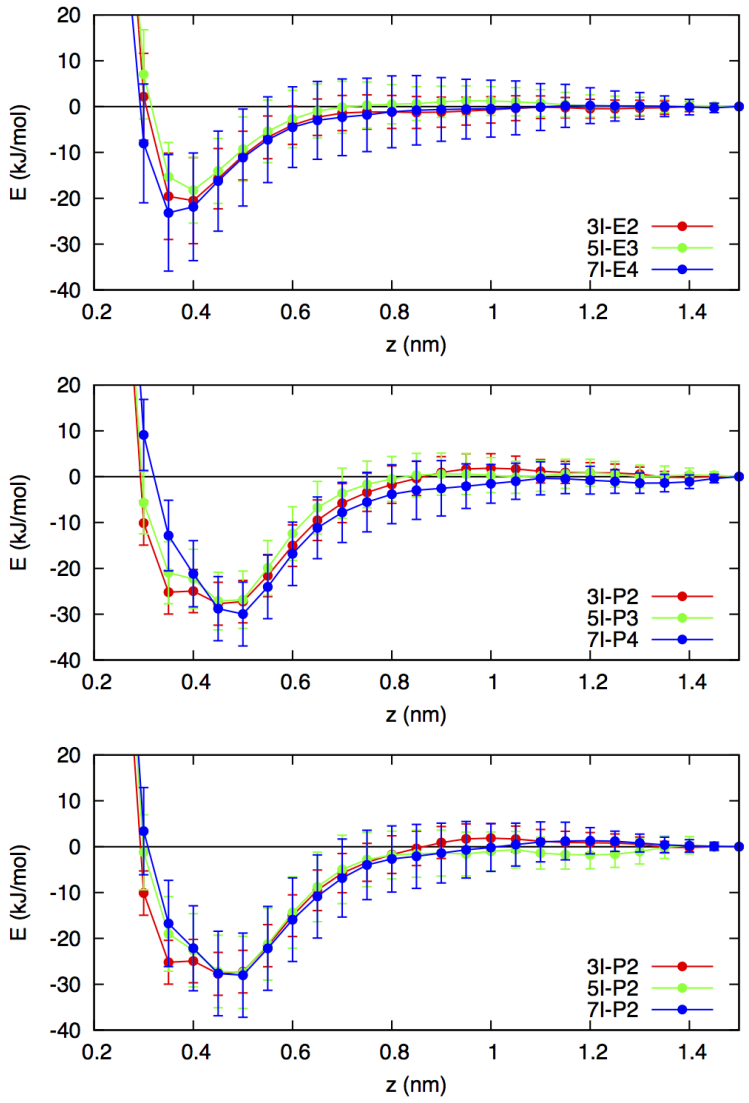

Figure 2: $V_{\text{eff}}(z)$ for (a) the central E bead, (b) the central P bead and (c) the second P bead (P2) in 3mer, 5mer and 7mer isotactic (I) oligomers.

The effective potentials for the central E bead are shown in Figure 2(a). Clearly for the three different chain lengths the potentials are very similar. Therefore we can conclude that the 3mer is sufficient for sampling the conformational space of the E beads.

The case of the *P* beads is different. The effective potentials for the central phenylene bead in

each oligomer is shown in Figure 2(b). There is a small difference in the shape of the three curves around 0.35 nm from the surface. To check that this is not due to poor sampling the calculations in the range 0.3-0.4 nm were extended to 100 ns and the results were very similar. Hence, this effect is likely to be due to long range correlations in the chain. This is not surprising if we consider that for the CG model it was necessary to take 1-5 interactions into account to obtain the correct local structure of the bulk PS chains. The shorter oligomers are missing the long range interactions which may result in different conformations with lower energy around 0.35 nm. To further check that this is the likely explanation, V_{eff} for the second phenylene bead (P2) in each oligomer was calculated. In the 5mer and 7mer chains the P2 bead has the same interactions up to the sixth nearest neighbor, compared to only the fourth nearest neighbour for the central bead. The effective potentials for the P2 bead are shown in Figure 2(c) and V_{eff} for the 5mer and 7mer agree.

Effect of tacticity and chain ends

Next we consider the effect of tacticity and bead position. This is particularly important if we consider that our PS CG model has the advantage of describing accurately the tacticity of PS bulk systems. Therefore, we would also like to calculate the PS/Au interaction for isotactic and syndiotactic PS chains. $V_{\text{eff}}(z)$ for all six beads in isotactic and syndiotactic trimers are shown in Figure 3 and the bead labelling is shown in the inset of Figure 3(a). All the ethylene beads have very similar effective potentials, as seen in Figure 3, and are only weakly dependent on tacticity and position. The strength of the interaction is around 20 kJ/mol, which is lower than the minimum energy of the vertical (27 kJ/mol) and horizontal (35 kJ/mol) configurations calculated using density functional theory.[13] The small difference is not surprising if we consider that the effective potentials explicitly incorporate thermal energy effects.

There is a clearer difference between the effective potentials for the phenylene beads. The phenylene ring at the end of the chain (P3) is independent of tacticity since the ring is free to rotate or exchange positions with the hydrogen atom. It has the strongest attraction of around 50 kJ/mol due to the fact that it is has fewer conformational constraints than more central beads. The phenyl

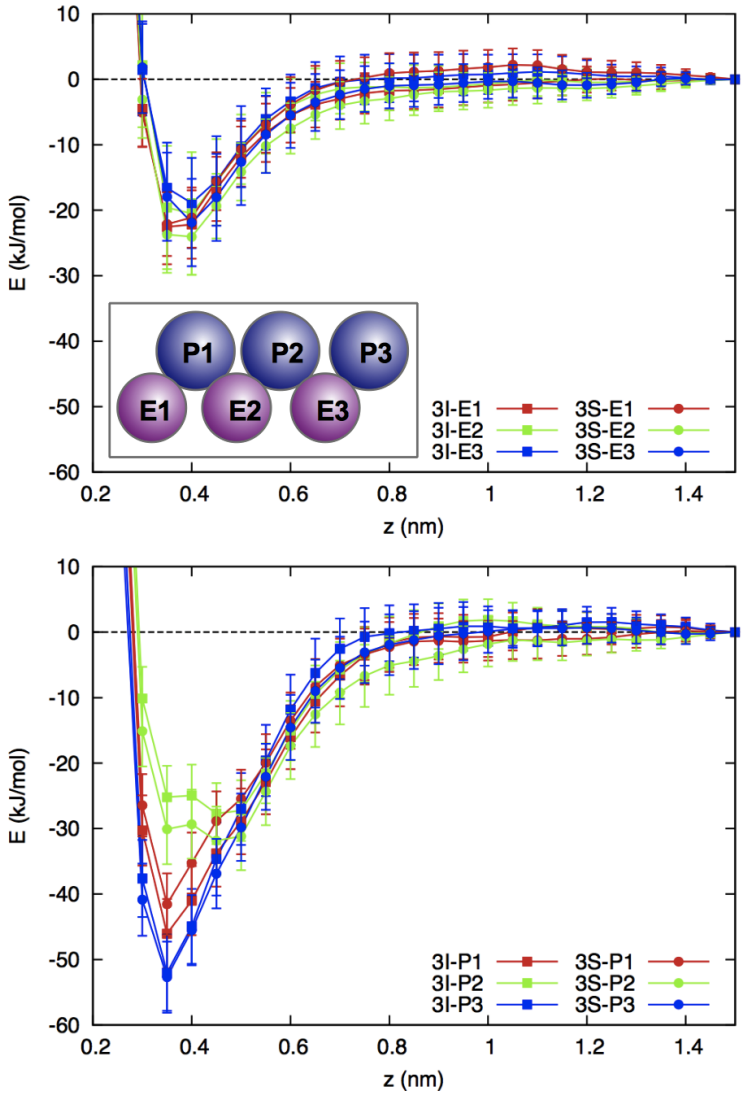

Figure 3: $V_{\text{eff}}(z)$ for (a) the ethylene beads and (b) the phenylene beads in an isotactic (I) and a syndiotactic (S) 3mer.

bead at the other end of the chain (P1) experiences some conformational constraints due to the end ethylene bead (E1) and therefore has a slightly weaker interaction of around 45 kJ/mol. The central bead (P2) is the most weakly attractive with a interaction of around 30 kJ/mol. The P1 and P2 beads exhibit only a small dependence on tacticity, which can be neglected.

We can further compare the $V_{\text{eff}}(z)$ curves with the interaction of benzene on a gold surface.[19] For benzene in a horizontal orientation the minimum energy is around 80 kJ/mol at distance of around 0.3 nm from the surface. The vertical configuration has a weaker interaction of around

30 kJ/mol at a distance of 0.5 nm. As expected, the effective potentials of the phenylene beads represent an average of these orientations due to thermal fluctuations. The chains ends are less constrained and, therefore, more likely to be in a horizontal orientation with a minimum energy around 0.35 nm from the surface. The central beads have more vertical or intermediate orientations with shallower minima further from the surface at around 0.45 nm.

A surface interaction of ≈ 30 kJ/mol corresponds to 7.2 kT at $T = 500$ K, which implies that once a bead becomes attached to the surface it remains at the surface for a long time. The bead–surface interactions are considerably stronger than the bead–bead non-bonded interactions within the bulk polymer. For the bulk polymer the non-bonded potentials are less than 3 kJ/mol deep, which is an order of magnitude weaker than the surface potentials. However, the surface potentials represent the interaction between the bead and many surface atoms, whereas the non-bonded potentials describe individual bead–bead interactions.

Fitting the potentials

For the E beads the effective potentials are very similar and we have chosen to represent all the E interactions with the same V_{eff}, namely the isotactic 3mer for the E2 bead. For the P beads it is clear that the interactions of the chain ends must be treated separately from the central beads and, therefore we have three different interactions for the P beads: P1 and P3 for the first and last P bead in each chain, respectively, and P2 (or P4 in the case of the 7mer) for all the others. Since the P1 and P3 beads do not depend much on tacticity we use the isotactic 3mer effective potentials for these beads. For the P2 bead it is not *a priori* clear whether it is best to use the 3mer or 7mer V_{eff} for the P2 bead (again we chose the isotactic chain), although the differences in the effective potentials are small and well within the expected error for CG simulations. Nevertheless, we decided to check whether the properties of the CG system depend on this choice. We also considered whether a simple analytical potential could be used to fit the original V_{eff} data or whether a numerical fit was

necessary. For the analytic potential we used a Morse-type potential of the form

$$V(z) = \varepsilon \{\exp[-2\alpha(z-z_0)] - 2\exp[-\alpha(z-z_0)]\} \quad (3)$$

where z is the distance to the surface and α, z_0 and ε are adjustable parameters. This analytic form was chosen because it was found to accurately describe the atomistic interface pair potentials for the PS–Au AA model systems.[13,19] The parameters that gave the best fit for the CG effective potentials are listed in Table 1.

Table 1: Morse parameters for each bead type in an isotactic 3mer. V_{eff} for the E2 bead in an isotactic 3mer was used for all E beads.

	ε	z_{equil}	α
3I-E2	20.22	0.3774	9.09
3I-P1	47.00	0.3638	7.73
3I-P2	31.90	0.3913	7.19
3I-P3	51.90	0.3491	8.47

The effective potential data and fitted potentials are shown in Figure 4. For the P2 bead we show both the 3mer and 7mer effective potentials, the cubic spline fits to the 3mer and 7mer and the Morse fit to the 3mer. It is clear that the Morse potential provides very good fits for the interaction between E, P1 and P3 beads and the Au surface, which all have a clear minimum. However, for the P2 bead in the 3mer the minimum has a shoulder around 0.35 nm and the Morse potential does not represent this very well. Therefore, all the V_{eff} curves were also fit using cubic splines (CS), implemented using the ALGLIB package.[23] The CS fitted potentials were then used in tabulated form. The sensitivity of the results to these three different sets of CG interface potentials is investigated in the following section. The sets are denoted as follows: a) M-3I-P2: Morse fits for the 4 bead types in an isotactic 3mer, b) CS-3I-P2: CS fits for the 4 bead types in an isotactic 3mer and c) CS-7I-P4: CS fits for E, P1 and P3 in an isotactic 3mer and P4 (for the central P beads) in an isotactic 7mer.

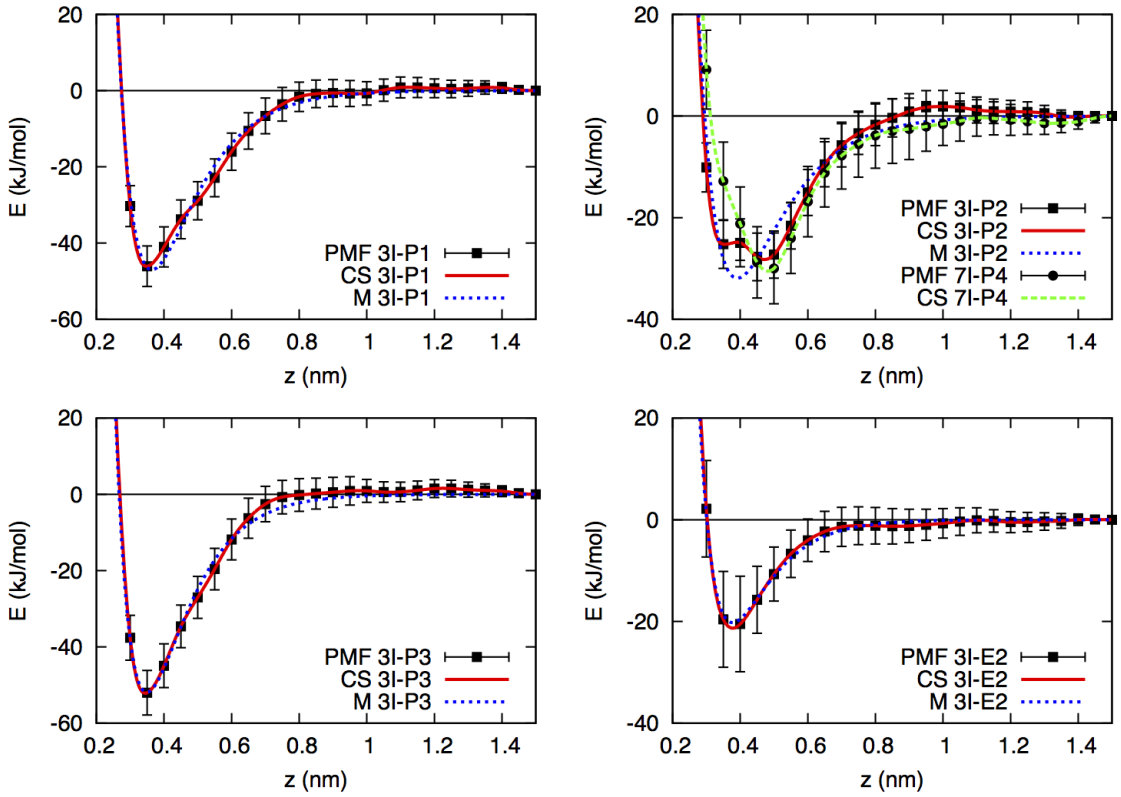

Figure 4: The effective potentials, fitted cubic splines and fitted Morse potentials for the four different CG bead types in an isotactic chain: a) 3I-P1, b) 3I-P2 and 7I-P4 c) 3I-P3 and d) 3I-E2.

Comparison between all-atom and coarse-grained simulations

To ensure that the CG model and potentials represent the system accurately, we begin with a detailed comparison of a short chain PS/Au system, which can be simulated using both CG and all-atom (AA) models. We chose a 5 nm 10mer PS/Au film, denoted S5-10, which was previously studied using all-atom MD simulations*. For the CG S5-10 systems a time step of 3 fs was used, which did not result in any significant difference from using a time step of 1 fs. A snapshot for this system is shown in Figure 5.

The averaged film properties for the S5-10 system, as well as the bulk systems, using the three different sets of potentials are given in Table 2. Both bulk systems and film contained 50 chains. For the CG bulk 10mer system the ensemble-averaged chain dimensions are $\langle R_g \rangle = 0.62$ nm and

*In the previous publication[13] the system was labelled S3 but in this paper we change the notation to S5-10, denoting the approximate film width and the number of monomers per chain.

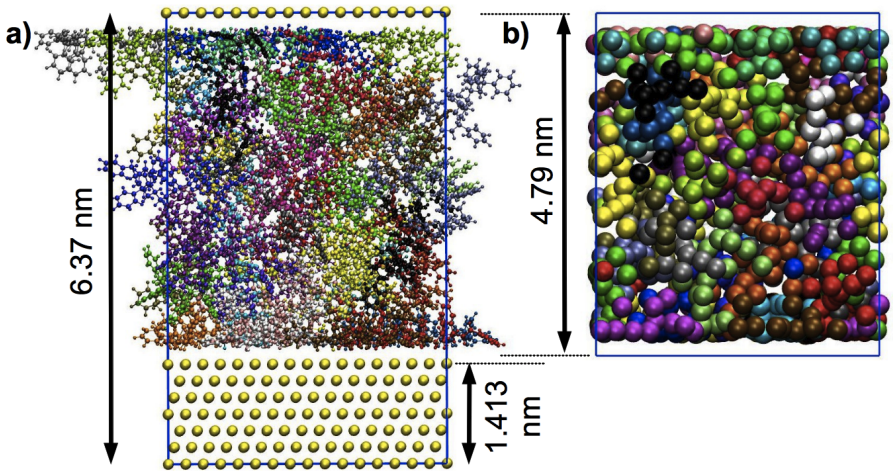

Figure 5: Snapshots of the CG S5-10 system with a) AA and b) CG representations. Each chain is represented with a different color.

Table 2: Summary of the 10mer film and bulk systems studied, the CG surface potentials used, and the average properties. The film thickness, L_z, and characteristic chain lengths, R_e and R_g, are in nm and the density, ρ, is in $g\,cm^{-3}$. The standard deviations of R_e and R_g are approximately 0.4 nm and 0.05 nm in all cases, respectively.

Model	Label	Fit	Potential	$\langle L_z \rangle$	$\langle \rho \rangle$	$\langle R_e \rangle$	$\langle R_g \rangle$
AA	B-10	-	-	-	0.97	1.57	0.63
CG	B-10	-	-	-	0.97	1.55	0.62
AA	S5-10	-	-	4.96	0.95	1.59	0.63
CG	S5-10	CS	3I-P2	4.79	0.98	1.65	0.63
CG	S5-10	CS	7I-P4	4.75	0.99	1.67	0.63
CG	S5-10	M	3I-P2	4.76	0.98	1.63	0.63

$\langle R_e \rangle = 1.55$ nm. To compare the CG system with the AA system we mapped the AA system to a CG representation and analyzed this in the same way as the CG systems. R_e shows the same trend for the AA and CG systems, that is, the S5-10 film has a higher value compared to the bulk system. R_g is almost the same for all the systems. In all systems the surface area of the simulation cell is the same so we can directly compare the film thicknesses and in future we can easily backmap from the CG to AA system. The film thicknesses are influenced not only by the average bulk density but also by the density at the surfaces. In the AA system the thickness of the PS film is defined as the cell length, L_z, minus the distance from the Au atom at the bottom of the slab at $z = 0$ nm to

the Au atom at the top of the slab at 1.413 nm. Note that this is a slightly different definition of the film width from that used in the previous publication,[13] where the PS film width was defined by subtracting off the thickness of seven atomic layers of gold, corresponding to 1.649 nm. The film thicknesses for all three CG potentials are only slightly smaller than the AA film thickness and the three different CG potentials have very similar average densities and film thicknesses.

Density profiles

To check that the CG systems give reasonable agreement with the AA systems we take the S5 system and compare the structural properties. The AA density profiles are symmetrized along the z-axis. The monomer and bead density profiles are shown in Figure 6(a) and (b), respectively. The monomer densities for the three CG systems are very similar. The position and height of the first density peak is in excellent agreement with the AA system. However the CG models all predict a second peak at around 0.6-0.7 nm, which is not visible in the AA system, and a deeper minimum than the AA system at around 0.8 nm. The bead density for the CG systems, in Figure 6(b), shows two clear peaks at the surface, compared with only one clear peak for the AA results, and the first peak for the CG system is rather higher than for the AA system.

To find the origin of this discrepancy, the density profiles for the individual bead types, i.e. E, P1, P2, and P3, were also calculated and are shown in Figure 7. The three CG systems and the AA system have almost identical bead density profiles for the E beads. The AA and CG profiles are very similar for P1 and P3, with the peaks in the same position but the height of the AA peaks being about half that of the CG peaks. However, for the central P beads (P2) the CG systems and the AA system are clearly different. All three CG systems have an inner peak at around 0.7 nm and additional peak (or plateau in the case of the CS-3I-P2 CG potential) around 0.3-0.5 nm. In contrast, the AA density profile for the P2 beads has a single peak at around 0.4-0.5 nm. This difference is a local effect that does not involve mass transfer towards the surface. This is clear from the density profile of the E beads, which is the same for the AA and CG systems.

The difference in the first peak or plateau of the P2 beads for the CG films is not surprising since

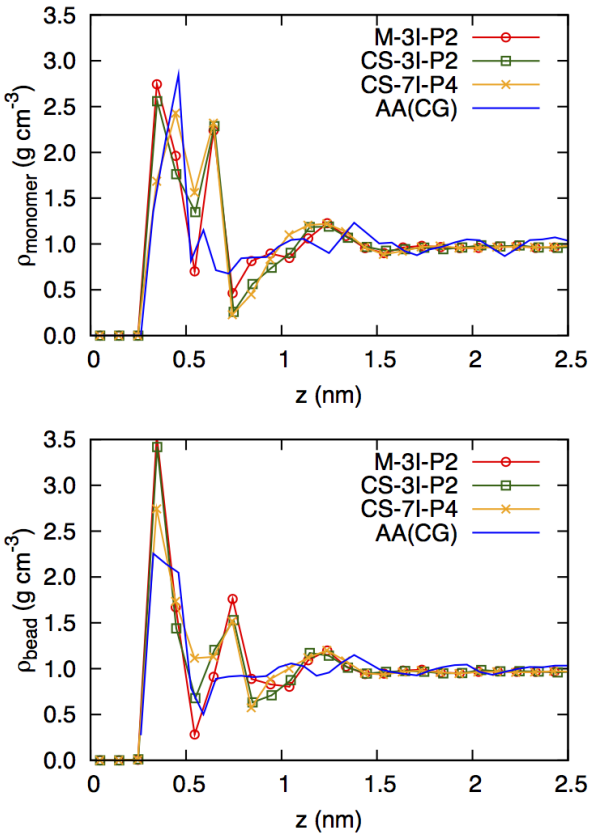

Figure 6: Monomer (top) and bead (bottom) density profiles for S5 films with the three CG interface potentials and the AA model (mapped to CG representation).

the main differences in the potentials is in the fitting of the central P bead, as shown previously in Figure 4. To check that the appearance of the strong second peak is not due to long-range correlations missed by using an oligomer to determine the effective potentials, we performed short simulations of 100 trimers between two gold surfaces. Similarly, the CG density profiles for the central P2 beads exhibit an inner peak that does not appear in the AA density profile. The density profiles for this system are shown in the supplementary information. The appearance of the strong second peak is likely to be a consequence of approximating the atomistic potentials by spherical CG potentials. It could also be in part due to the slightly different angular distributions between the AA and CG models.

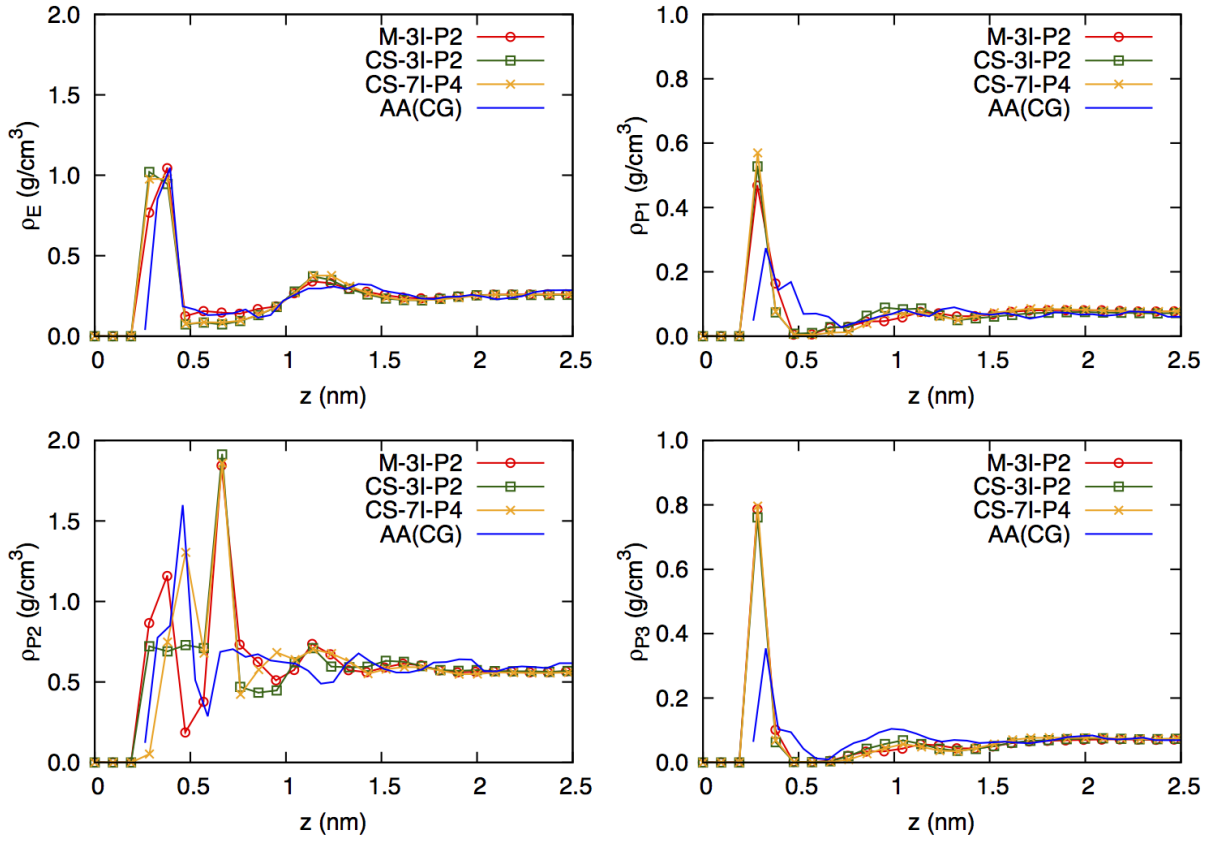

Figure 7: Bead density profiles for the CG and AA S5 films for each bead type (a) E, (b) first phenylene group (P1), (c) all central phenylene groups (P2) and (d) the terminal phenylene group (P3).

Bond order

The structure of the polymer–metal interfaces can be directly studied through a vector order parameter. Here, we use the bond order parameter P_2, which is defined as

$$P_2 = \frac{3}{2}\langle \cos^2 \theta \rangle - \frac{1}{2} \tag{4}$$

We investigate the bond order profiles for the AA system and the three CG systems. As before, the AA system was mapped to the CG representation for analysis and symmetrised along the z-axis. First we look at the bond order parameter for the vector E–P, shown in Figure 8a). As shown in the previous paper,[13] the order parameter next to the surface is close to -0.5, which corresponds to the vectors lying parallel to the surface. A similar behaviour is seen for the bond order parameter

E–E, which corresponds to the backbone, shown in Figure 8b). In both cases there is almost no difference between the three CG systems and the AA system.

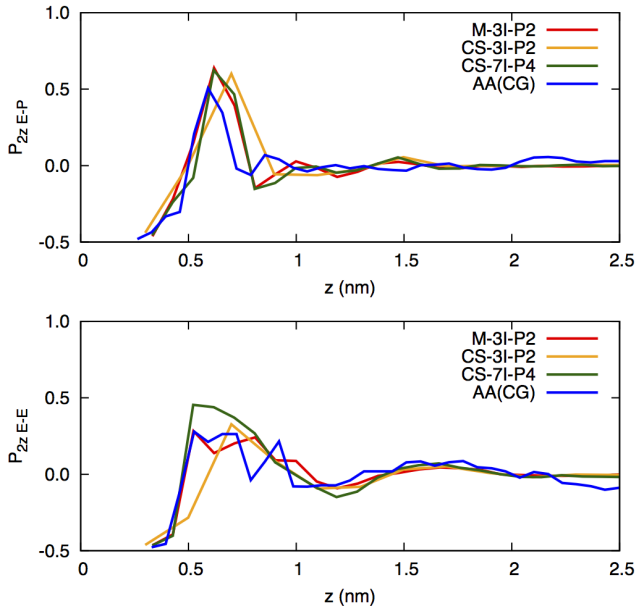

Figure 8: Bond order profiles for the S5 system using the AA and CG models. The top graph shows the bond order parameter for the vector E–P within the same monomer and the lower graph for the vector E–E in adjacent monomers.

Chain conformations

The conformation of the chains in the films is compared by analyzing the conformation tensor along the z direction with a bin size of roughly 0.5 nm. The conformation tensor is defined as

$$\mathbf{C}_{\alpha\beta} = 3\frac{\langle R_{\mathrm{e}\,\alpha} R_{\mathrm{e}\,\beta}\rangle}{\langle R^2_{\mathrm{e\ bulk}}\rangle} \tag{5}$$

so that for a homogeneous system the conformation tensor is equal to the identity matrix. The conformation tensor profiles perpendicular to the plane, $\mathbf{C}_{zz}$ and parallel to the plane, $\mathbf{C}_{\mathrm{par}} = \frac{1}{2}(\mathbf{C}_{xx} + \mathbf{C}_{yy})$, are shown in Figure 9. The AA profile was mapped to the CG representation and symmetrized in the z-direction. The CG data is unsymmetrized. It is clear that the chains at the surface are flattened in z and elongated in the surface plane, which is typical behaviour for poly-

mers at solid surfaces. In addition, all three CG potentials give very similar conformation tensor profiles and are in excellent quantitative agreement with the AA system.

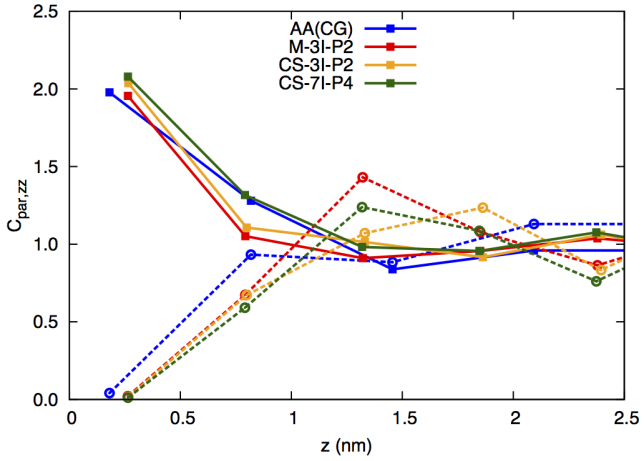

Figure 9: Conformation tensor profiles for the S5 system using the AA and CG models. $\mathbf{C}_{\text{par}}$ is shown with solid squares and solid lines and $\mathbf{C}_{zz}$ is shown with open circles and dashed lines.

Coarse-grained simulations of long-chain polystyrene films

Overall, it is clear that there is very good agreement between the AA and CG PS/Au systems concerning the structural properties of the interfaces for all CG PS/Au interaction potentials. Now we turn to larger systems with longer polymer chains and use the CS-3I-P2 potential. We consider PS films roughly 10 and 20 nm thick with 10mer, 50mer, 100mer and 200mer chains. For the systems with longer chain the surface area of the simulation cell is increased to avoid the polymer interacting with its own periodic image. The box length is set to be a multiple of the Au surface unit cell so that the system can be backmapped to the atomistic level. The box size is fixed in x and y throughout the simulation but allowed to vary in the z direction.

Equilibration of long-chain polymers is not a trivial issue. One measure of equilibration is when the end-to-end distance vectors R_{e} have decorrelated.[24,25] At 500 K this happens in less than a nanosecond for bulk 10mer systems and around 20-30 ns for the 10mer thin films. For longer-chain systems the time to decorrelation at 500 K is much longer and it is necessary to heat the system until R_{e} is decorrelated and then cool it back to 500 K. For the 50mer and 100mer systems the annealing

temperature was 800 K and for the 200mer systems the annealing temperature was 1000 K. Two different cooling rates were tested, a) $\Gamma = 10$ K/ns and b) $\Gamma = 1$ K/ns. After cooling to 500 K the systems were run for a further 100 ns before statistics were taken. No systematic dependences of the properties on cooling rate was observed. The internal distances, $\langle R^2(N)/N \rangle$, of each system were calculated to check that there was no residual strain in the chain. The decorrelation times and internal distances can be found in the supplementary information. All CG simulations were NpT with $p = 1$ atm and $T = 500$ K and were run for 500 ns, after equilibration. Note that the time here refers to coarse-grained time, which is faster than the real or atomistic time due to the reduced friction of the smoother energy landscape.

Average film properties

The ensemble-averaged film properties are shown in Table 3. Only the data for the fast-cooled films is shown here but the data for the slow-cooled films are given in the supplementary information. There is no significant change in average properties between 10 and 20 nm films. For all chain lengths R_e and R_g are slightly larger in the films than in the bulk. To investigate further the differences it is necessary to look at the various properties as a function of distance from the surface.

Density

The bead density profiles of the films are shown in Figure 10. For 10 and 20 nm films and all chain lengths the bead density profiles are indistinguishable. Similar to the S5 CG systems there are three visible peaks in the density at the surface and the profile reaches the bulk value around 1.5-2 nm.

The partial density profiles for the S10-10 and S10-200 films are shown in Figure 11. The partial densities for the S20 films are virtually identical to the S10 films. The first peak is composed of both P and E beads. For the 10mer film the contribution of P beads is higher than for the E beads but for the 200mer film the contributions are approximately equal. The 50mer and 100mer films

Table 3: Summary of the CG systems studied and their averaged properties. N_{chain} is the number of chains of N monomers. L_x, L_z, R_e and R_g are in nm and the average density ρ is in g cm^{-3}. The bulk systems are in cubic boxes with $L_x = L_y = L_z$ so only $\langle L_z \rangle$ is given. For the slabs the box is hexagonal with $L_y = \sqrt{3}L_x/2$, so only L_x (fixed) and $\langle L_z \rangle$ are given.

Label	N	N_{chain}	L_x	$\langle L_z \rangle$	$\langle \rho \rangle$	$\langle R_e \rangle$	$\langle R_g \rangle$
B-10	10	50	-	4.47	0.967	1.55	0.62
S20-10	10	200	4.616	19.34	0.969	1.58	0.62
S10-10	10	100	4.616	9.64	0.972	1.61	0.62
S5-10	10	50	4.616	4.79	0.978	1.65	0.63
B-50	50	50	-	7.50	1.025	3.89	1.62
S20-50	50	100	6.347	24.18	1.025	3.86	1.62
S10-50	50	50	6.347	12.10	1.024	3.92	1.64
B-100	100	50	-	9.42	1.033	5.61	2.38
S20-100	100	100	9.232	22.70	1.032	5.57	2.40
S10-100	100	50	9.232	11.37	1.031	5.63	2.42
B-200	200	50	-	11.86	1.037	8.16	3.43
S20-200	200	100	12.694	23.93	1.036	7.96	3.36
S10-200	200	50	12.694	11.99	1.033	8.19	3.48

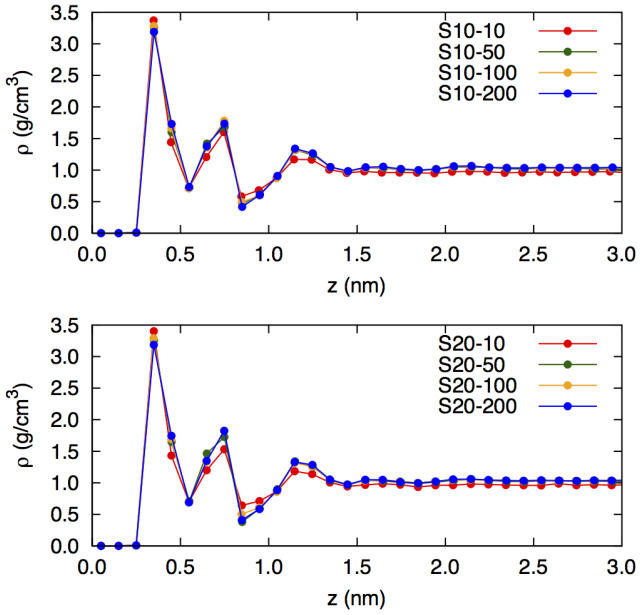

Figure 10: CG superatom density profiles for the S10 and S20 films.

are similar to the 200mer film. In all films the second peak is entirely due to P beads. This implies that the backbone is lying along the surface with some P superatoms alongside but the other P superatoms forming the next density layer. The next backbone layer occurs at around 1.2-1.3 nm

from the surface.

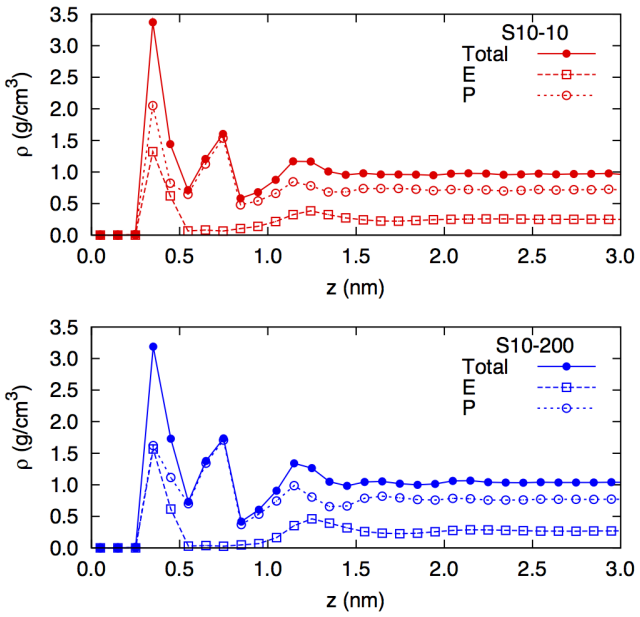

Figure 11: CG partial density profiles for the S10-10 (top) and S10-200 (bottom) films, showing the superatom P and E contributions.

Bond order

Since the statistics for the CG system are better than for the AA system it is possible to analyze bond order using smaller bin sizes. We have calculated the profiles for four different vectors: E-P, E-E, P-E and P-P. It is clear that at the surface the bond order parameters for all vectors are almost -0.5, indicating that the bonds are flat along the surface. As expected, the profiles for E-P and P-E are very similar. These profiles have a peak at around 0.5 nm, which implies a tendency for the bonds to be perpendicular, then are approximately zero after 0.8 nm. The E-E bond vector has a slightly lower but broader peak at 0.5-0.7 nm. These peaks correspond to the density minima at 0.5 nm, see Figure 10, and, therefore, this reflects the bonds connecting E beads in the first layer with P beads in the second layer. The P-P bond order parameter profile is qualitatively different to the other vectors and does not have a peak at 0.5 nm. Instead, it approaches zero at around 0.5 nm, indicating random orientation, becomes negative again indicating a weak preference for parallel orientation and becomes approximately random again after 1 nm.

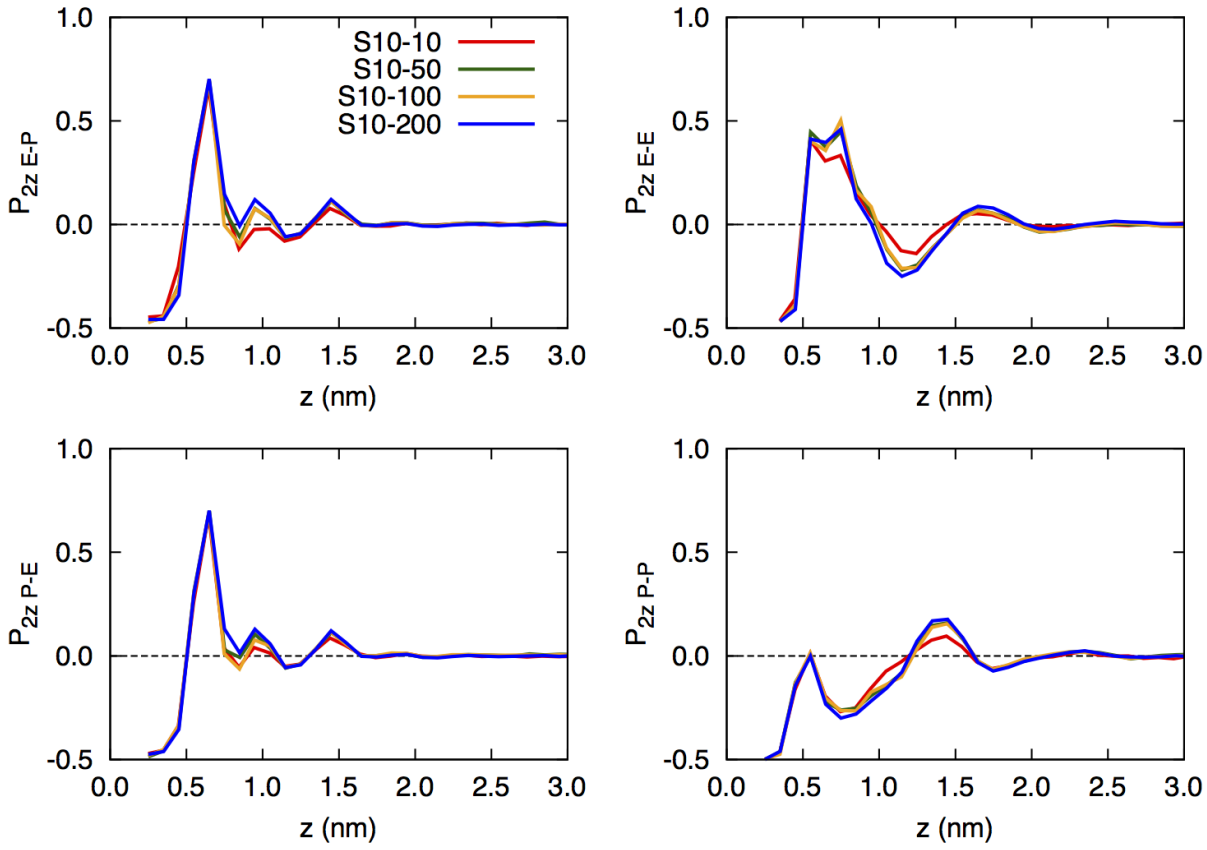

Figure 12: Bond order parameter profiles for the vectors E-P (top left), E-E (top right), P-E (bottom left) and P-P (bottom right).

Conformation tensor

To analyse the conformation tensor the average mean square end-to-end distance $\langle R_e^2 \rangle$ of the two bulk runs (with different cooling rates) was used and the symmetrised conformation tensor profiles are shown in Figure 13.

It is clear that in all films the chains nearest the surfaces are compressed in the z-direction. The in-plane component of the tensor is rather noisier and shows a much large fluctuation near the surface. In particular, in the S20-100 system the value at the surface is close to 1.0, which is considerably lower than the other films. This noise is due to the fact that the films are quite immobile near the surface and, in addition, the 100- and 200mer chains in bulk do not fully decorrelate within 500 ns at 500 K. Therefore the films are likely to be dependent on the setup. To check if this is the case an independent S20-100 system was set up for both cooling rates and the conformation

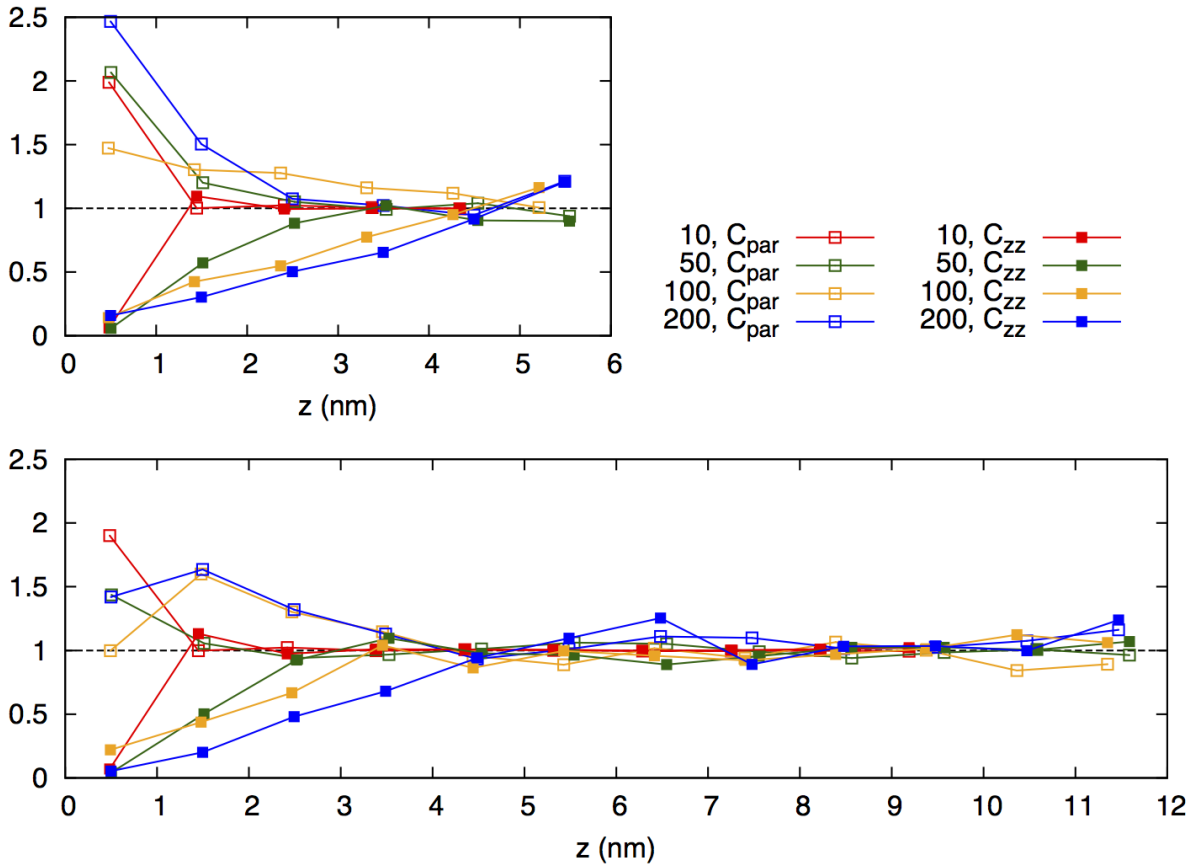

Figure 13: Conformation tensor profiles for S10 (top) and S20 (bottom) films. The data has been symmetrized and the in-plane component, $\mathbf{C}_{\text{par}}$, has been averaged over the x and y directions.

tensor $\mathbf{C}_{\text{par}}$ had values of 2.7 and 3.6 at the surface for the fast and slow cooling rates, respectively, which is within the statistical error bars.

Interphase width

It is well known that the interphase width is non-unique and is property specific. From the above analysis we can estimate the width of the interphase, W, and its dependence on chain length.

The density profiles for all films are almost identical and reach a bulk value at around $W_\rho = 1.5$ nm, which is independent of chain length. This is similar to the value of 1-2 nm that was observed previously in studies of 10-mer PS on silica nanoparticles[26] and 80-mer PS on a non-specific surface.[9] The bond order parameters become random at around $W_{P_{2z}} = 2$ nm, which is also independent of chain length. Clearly, since these are segmental quantities, the interphase

width measured in this way is independent of the chain length.

However, the distance at which the conformation tensor profile reaches its bulk behaviour is not chain length independent, as can be seen in Figure 13. W_C is estimated using the $\mathbf{C}_{zz}$ profiles since they are less noisy than $\mathbf{C}_{par}$. To improve statistics all data for both 10 and 20 nm films and both cooling rates was fitted. The conformation tensor profiles were fitted using a hyperbolic tangent of the form

$$\mathbf{C}_{zz}(z) = \tanh(z/A)$$

and this was used to estimate the interface width by calculating the value of z at which $\mathbf{C}_{zz}$ reached 0.95 and 0.98. Further details of the fitting procedure are given in the supplementary information. The interphase width estimates are plotted in Figure 14. For comparison we have plotted R_g and

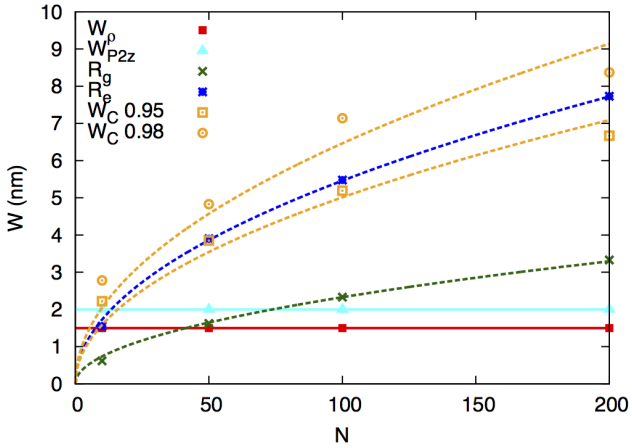

Figure 14: Dependence of estimated interphase width on chain length using density profiles, bond order profiles and conformation tensor profiles. For comparison R_g and R_e for the bulk systems is also plotted. The dashed lines are fits to the data of the form $kN^{\frac{1}{2}}$.

R_e for the bulk systems. The lines show the fits to the data of the form

$$W(N) = kN^{\frac{1}{2}}$$

and it is clear that R_g and R_e vary with $N^{\frac{1}{2}}$. The estimated interphase width W_C more closely follows R_e than R_g. A previous study using a generic CG model analysed the components of R_g and found that they reached the bulk value after a distance of R_g from the surface.[27]

Summary and Conclusions

A coarse-grained model for polystyrene on a gold surface was developed and used to investigate the structure of polystyrene films confined between parallel gold surfaces. The method used a hierarchical multiscale modelling approach where the surface interaction is based on density functional theory calculations and all-atom molecular dynamics simulations. The interface potentials were validated by comparing the coarse-grained and all-atom structures of a 5 nm thick 10mer polystyrene film on gold. The density and conformational properties using the all-atom and coarse-grained model were found to be in good agreement.

The structural properties of 10mer to 200mer polystyrene films roughly 10 and 20 nm thick confined between gold surfaces were then investigated using the coarse-grained model. The density profile at the interface was analyzed and it was found that both film thickness and all chain lengths gave indistinguishable profiles. The density reached the bulk value at around 1.5 nm from the surface. The conformation of the films was also analyzed and the distance from the interface where the bulk value was reached was found to be proportional to the square root of the chain length. For 200mer chains, the longest chain length studied here, the interphase width is estimated to be between $6-9$ nm, which is similar to the average end to end distance. Clearly, the interphase width and its variation with chain length depends on the property that is measured. The width of the interphase based on polymer dynamics should also be investigated but this is a topic for a future article.

Acknowledgements

We would like to thank Sebastian Fritsch and Dominik Fritz for valuable help and Kurt Kremer and Christine Peter for useful discussions and critical reading of the manuscript. This work was supported by the German Research Foundation (DFG) grant SPP 1369 "Interfaces and interphases". Partially supported by the European Union's Seventh Framework Programme (FP7-REGPOT-2009-1) project "Archimedes Center for Modeling, Analysis and Computation".

Supporting Information Available

References

(1) Koo, J. *Polymer Nanocomposites: Processing, Characterization, And Applications*; McGraw-Hill, 2006.

(2) Kim, H.; Abdala, A. A.; Macosko, C. W. *Macromolecules* **2010**, *43*, 6515.

(3) Priestley, R. D.; Ellison, C. J.; Broadbelt, L. J.; Torkelson, J. M. *Science* **2005**, *309*, 456.

(4) Qi, D.; Fakhraai, Z.; Forrest, J. A. *Phys. Rev. Lett.* **2008**, *101*, 096101.

(5) Tress, M.; Erber, M.; Mapesa, E. U.; Huth, H.; Mueller, J.; Serghei, A.; christpph Schick,; Eichhorn, K.-J.; Voit, B.; Kremer, F. *Macromolecules* **2010**, *43*, 9937.

(6) Hoppe, E. T.; Hopp, I.; Port, M.; Menges, B.; Papadakis, C. M. *Colloid Polym. Sci.* **2012**, *290*, 1731.

(7) Doi, M.; Edwards, S. F. *The Theory of Polymer Dynamics*; Clarendon Press: Oxford, England, 1986.

(8) Borodin, O.; Smith, G. D.; Bandyopadhyaya, R.; Byutner, O. *Macromolecules* **2003**, *36*, 7873.

(9) Hudzinskyy, D.; Lyulin, A. V.; Baljon, A. R. C.; Balabaev, N. K. B. K.; Michels, M. A. J. *Macromolecules* **2011**, *44*, 2299.

(10) Yelash, L.; Virnau, P.; Binder, K.; Paul, W. *Europhysics Letters* **2012**, *98*, 28006.

(11) Harmandaris, V. A.; Daoulas, K. C.; Mavrantzas, V. G. *Macromolecules* **2005**, *38*, 5796.

(12) Yelash, L.; Virnau, P.; Binder, K.; Paul, W. *Phys. Rev. E* **2010**, *82*, 050801.

(13) Johnston, K.; Harmandaris, V. *Soft Matter* **2012**, *8*, 6320–6332.

(14) Abrams, C. F.; Kremer, K. *Macromolecules* **2003**, *36*, 260.

(15) Villa, A.; Peter, C.; van der Vegt, N. F. A. *Phys. Chem. Chem. Phys.* **2009**, *11*, 2077.

(16) Fritz, D.; Harmandaris, V. A.; Kremer, K.; van der Vegt, N. F. A. *Macromolecules* **2009**, *42*, 7579.

(17) Delle Site, L.; Abrams, C. F.; Alavi, A.; Kremer, K. *Phys. Rev. Lett.* **2002**, *89*, 156103.

(18) Johnston, K.; Nieminen, R. M.; Kremer, K. *Soft Matter* **2011**, *7*, 6457–6466.

(19) Johnston, K.; Harmandaris, V. *J. Phys. Chem. C* **2011**, *115*, 14707.

(20) Hess, B.; Kutzner, C.; van der Spoel, D.; Lindahl, E. *Journal of Chemical Theory and Computation* **2008**, *4*, 435–447.

(21) Müller-Plathe, F. *Macromolecules* **1996**, *29*, 4782.

(22) Harmandaris, V. A.; Reith, D.; van der Vegt, N. F. A.; Kremer, K. *Macromol. Chem. Phys.* **2007**, *208*, 2109.

(23) Bochkanov, S.; Bystritsky, V. ALGLIB. `http://www.alglib.net/`.

(24) Mavrantzas, V. G.; Boone, T. D.; Zervopoulou, E.; Theodorou, D. N. *Macromolecules* **1999**, *32*, 5072.

(25) Auhl, R.; Everaers, R.; Grest, G. S.; Kremer, K.; Plimpton, S. J. *J. Chem. Phys.* **2003**, *119*, 12718.

(26) Ndoro, T. V. M.; Voyiatzis, E.; Ghanbari, A.; Theodorou, D. N.; Böhm, M. C.; Müller-Plathe, F. *Macromolecules* **2011**, *44*, 2316.

(27) Virgilis, A. D.; Milchev, A.; Rostiashvili, V. G.; Vilgis, T. A. *Eur. Phys. J. E* **2012**, *35*, 97.

This material is available free of charge via the Internet at `http://pubs.acs.org/`.